

# On Reciprocity in Physically Consistent TDD Systems with Coupled Antennas

Tobias Laas, *Graduate Student Member, IEEE*, Josef A. Nossek, *Life Fellow, IEEE*, Samer Bazzi, and Wen Xu, *Senior Member, IEEE*

**Abstract**—We consider the reciprocity of the information-theoretic channel of Time Division Duplex (TDD) Multi-User-Multiple Input Multiple Output (MU-MIMO) systems in the up- and downlink. Specifically, we assume that the transmit and receive chains are reciprocal. We take the mutual coupling between the antenna elements at the base station and at the mobiles into account. Mutual coupling influences how to calculate transmit power and noise covariance. The analysis is based on the Multiport Communication Theory, which ensures that the information-theoretic model is consistent with physics. It also includes a detailed noise model. We show that due to the coupling, the information-theoretic up- and downlink channels do not fulfill the ordinary reciprocity relation, even if the input-output relation of the transmit voltage sources and the receive load voltages, i.e., the channel which is estimated with the help of pilot signals in the uplink, is reciprocal. This is a fundamental effect that is not considered otherwise. We show via Monte Carlo simulations that both, using the ordinary reciprocity relation, and not taking the coupling into account, significantly decreases the ergodic rates in single-user and the ergodic sum rates in multi-user systems.

**Index Terms**—Wireless communication, reciprocity, MIMO systems, multiport communication theory, smart antennas.

## I. INTRODUCTION

CURRENTLY deployed wireless standards such as LTE only employ a small number of antennas at the mobiles and at the base station. It is expected that to accommodate further growth of the amount of transferred data, a significantly larger number of antennas needs to be employed at the base station. In order to exploit the degrees of freedom provided by the antennas, the base station requires channel state information (CSI). The amount of CSI increases with the number of antennas. In frequency division duplex (FDD) mode, the base station can usually acquire downlink CSI by sending pilot signals, letting the mobiles estimate the CSI and feed back the estimate. The advantage of time division duplex (TDD) mode is that the base station can reuse CSI from the uplink,

This work has been partly performed in the framework of the Horizon 2020 project ONE5G (ICT-760809) receiving funds from the European Union. This paper was presented in part at the 21st International ITG Workshop on Smart Antennas (WSA), Berlin, Germany, March 2017.

T. Laas is with the German Research Center, Huawei Technologies Duesseldorf GmbH, 80992 Munich, Germany, and also with the Department of Electrical and Computer Engineering, Technical University of Munich, 80333 Munich, Germany (e-mail: tobias.laas@tum.de).

J. A. Nossek is with the Department of Electrical and Computer Engineering, Technical University of Munich, 80333 Munich, Germany, and also with the Department of Teleinformatics Engineering, Federal University of Ceará, Fortaleza, Brazil (e-mail: josef.a.nossek@tum.de).

S. Bazzi and W. Xu are with the German Research Center, Huawei Technologies Duesseldorf GmbH, 80992 Munich, Germany (e-mail: samer.bazzi@huawei.com; wen.xu@ieee.org).

as the physical channel is reciprocal [1]. The uplink CSI can be acquired with less pilot overhead than the downlink CSI if there are in total fewer antennas at the mobiles than at the base station.

In practical systems, the transmit (Tx) and receive (Rx) RF chains are usually not identical, i.e., up- and downlink channels are not reciprocal. Reciprocity calibration is used to take this into account [2], [3], [4], [5], [6], [7]. In some of these papers, the mutual coupling between the antenna elements of the same array is leveraged for the calibration process. But they do not take into account that mutual coupling itself has an impact on the reciprocity relation of the up- and downlink channel matrices in the information-theoretic model. Here we assume that one of the methods for calibrating the RF chains is applied such that those in the uplink and those in the downlink are made equal in the DSP part of the system.

We will show that there is another fundamental source changing the reciprocity relation, namely mutual coupling, using the so-called Multiport Communication Theory [8], [9]. This theory is in turn based on a circuit-theoretical description using impedance matrices and provides a way to model the system consistently with physics. The circuit model can equivalently be described using scattering matrices, similar to the models [10], [11], which to the authors' best knowledge were the first to take into account that mutual coupling changes the transmit power. The model in [10] was later extended by a detailed amplifier noise model [12]. Two similar noise models that contain both antenna and amplifier noise are introduced in [8], [9], and [13]. The key contributions of [8] and [9] are that it merges the circuit model and the noise model, and that it introduces a systematic mapping from the circuit-based models to the usual information-theoretic model. All of these models only consider a one-way link, so it is applied to both up- and downlink in analyzing reciprocity. In conventionally modeled systems, the information-theoretic ordinary (pseudo-physical) reciprocity relation  $\mathbf{H} = \mathbf{H}_{\text{UL}}^T$  is employed, but due to mutual coupling, this relation does not hold, but rather a new physically consistent reciprocity relation. This is because mutual coupling influences how to calculate transmit power and noise covariance.

The rest of the paper is organized as follows: first we review a simple circuit-theoretic model in Section II, then we consider the reciprocity of the information-theoretic channel and show how to take it into account in Section III. We analyze the effect on the radiated power and on the (sum) rates in the single user multiple input single output (SU-MISO), single user multiple input multiple output (SU-MIMO), multi user MISO

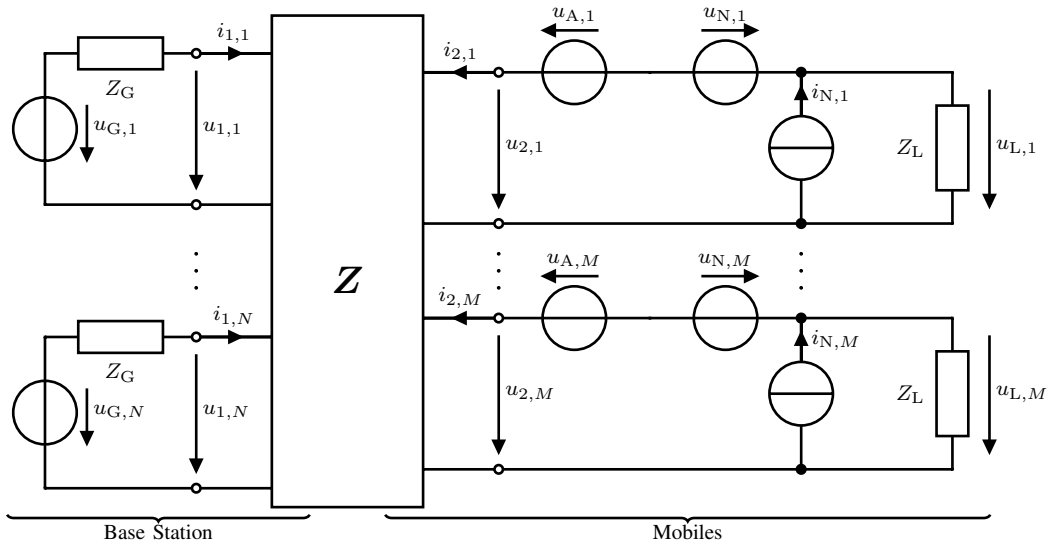


Fig. 1. Circuit model in the downlink.

(MU-MISO) and MU-MIMO downlink, first theoretically, see Section IV, and second in simulation in independent and identically distributed (i.i.d.) channels and in QuaDRiGa [14], [15] channels, see Sections V and VI. The SU-MISO case was presented in part in a conference paper [16]. Conclusions follow in Section VII.

*Notation:* lowercase bold letters denote vectors, uppercase bold letters matrices.  $a_m$  denotes the  $m$ th element of  $\mathbf{a}$ .  $\mathbf{A}^T$ ,  $\mathbf{A}^*$ ,  $\mathbf{A}^H$ ,  $|\mathbf{A}|$ ,  $\|\mathbf{A}\|_F$ ,  $\text{tr}(\mathbf{A})$  and  $\text{diag}(\mathbf{A})$  correspond to the transpose, the complex conjugate, the Hermitian, the determinant, the Frobenius norm, the trace and the matrix whose diagonal elements are equal to those of  $\mathbf{A}$  and whose other entries are zero.  $\mathbf{0}$  and  $\mathbf{I}$  denote zero vector and identity matrix.  $\mathcal{N}_C(\boldsymbol{\mu}, \mathbf{R})$  denotes a proper complex Gaussian distribution with mean  $\boldsymbol{\mu}$  and covariance  $\mathbf{R}$ .  $\mathbb{E}[X]$  denotes the expectation of the random variable  $X$ .

## II. MULTIPORT COMMUNICATION THEORY

### A. Circuit-Theoretic Model

We focus on a simple circuit model (Fig. 1) for the fading channel by assuming that the fading is flat within a narrowband (group of) subcarrier(s) of a multicarrier system<sup>1</sup>, similar to the ones in [8], [9, Fig. 9] and [17], [18], where simple means that as in [17], [18], we omit the lossless decoupling and impedance matching network (DMNs), because in massive MIMO systems, they could be almost impossible to implement. But as in [8], [9] and [18], we also consider the thermal noise of the antennas.

The signal generation at the transmitter is modeled as a linear voltage source  $u_{G,n}$  with internal impedance  $Z_G$  per antenna. The antennas are assumed to be lossless [9] and their coupling and the physical channel are modeled jointly by an impedance matrix  $\mathbf{Z}$ . At the receivers, each hardware chain is modeled by an impedance  $Z_L$  and several noise sources, which we will come back to later.

<sup>1</sup>This is the standard assumption in most of the MIMO literature.

Let there be in total  $N$  antennas at the transmitter(s) and  $M$  at the receiver(s). As antennas and the physical channel are reciprocal [19], the system described by the impedance matrix  $\mathbf{Z} \in \mathbb{C}^{(N+M) \times (N+M)}$ .  $\Omega$  is reciprocal as well, i.e.,

$$\mathbf{Z} = \mathbf{Z}^T. \quad (1)$$

It is partitioned into four blocks [8]: the transmit and receive impedance matrices  $\mathbf{Z}_{11} \in \mathbb{C}^{N \times N}$ .  $\Omega$  and  $\mathbf{Z}_{22} \in \mathbb{C}^{M \times M}$ .  $\Omega$ , and the mutual impedance matrices  $\mathbf{Z}_{21} \in \mathbb{C}^{M \times N}$ .  $\Omega$  and  $\mathbf{Z}_{12} \in \mathbb{C}^{N \times M}$ .  $\Omega$  such that

$$\begin{bmatrix} \mathbf{u}_1 \\ \mathbf{u}_2 \end{bmatrix} = \underbrace{\begin{bmatrix} \mathbf{Z}_{11} & \mathbf{Z}_{12} \\ \mathbf{Z}_{21} & \mathbf{Z}_{22} \end{bmatrix}}_{\mathbf{Z}} \begin{bmatrix} \mathbf{i}_1 \\ \mathbf{i}_2 \end{bmatrix}, \quad (2)$$

where  $\mathbf{u}_1 \in \mathbb{C}^N \cdot \text{V}$ ,  $\mathbf{i}_1 \in \mathbb{C}^N \cdot \text{A}$ ,  $\mathbf{u}_2 \in \mathbb{C}^M \cdot \text{V}$ ,  $\mathbf{i}_2 \in \mathbb{C}^M \cdot \text{A}$  are the port voltages and currents at the transmitter and receiver side [8] (see Fig. 1). All voltages and currents in this paper are rms values of complex envelopes.

Let us consider the relation between the generator and load voltages  $\mathbf{u}_G \in \mathbb{C}^N \cdot \text{V}$  and  $\mathbf{u}_L \in \mathbb{C}^M \cdot \text{V}$ . Compared to [8], the relation between voltages and currents at the generator side simplifies to

$$\mathbf{u}_G = \mathbf{u}_1 + Z_G \mathbf{i}_1. \quad (3)$$

Using the unilateral approximation  $\|\mathbf{Z}_{12}\|_F \ll \|\mathbf{Z}_{11}\|_F$  [8], whereby we assume that the attenuation of the channel is so high that the currents in the antennas at the receivers do not influence the transmitter, we have [8]

$$\mathbf{u}_1 = \mathbf{Z}_{11} \mathbf{i}_1. \quad (4)$$

According to the superposition theorem,

$$\begin{aligned} \mathbf{u}_L &= \underbrace{\mathbf{u}_L|_{\text{nf}}}_{\text{noise-free}} + \underbrace{\mathbf{u}_L|_{\text{sf}}}_{\text{signal-free}} \\ &= \mathbf{u}_L|_{\text{nf}} + \sqrt{R_L} \boldsymbol{\eta}, \quad R_L := \text{Re}(Z_L), \end{aligned} \quad (5)$$

where  $\boldsymbol{\eta}$  describes the noise and will be given in (12).

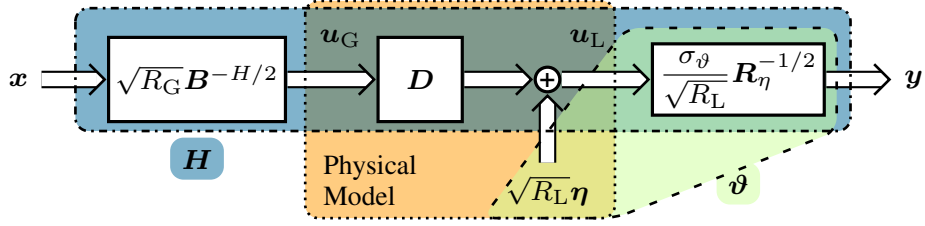


Fig. 2. System model showing the relation between the physical and the information-theoretic model.

The excitation in the noise-free case is caused by  $\mathbf{u}_G$ , and in the signal-free case by the noise sources. We use the same noise model as in [9], which distinguishes between the extrinsic noise  $\mathbf{u}_A \in \mathbb{C}^M \cdot \mathbf{V}$  produced by the antennas in thermal equilibrium, and the intrinsic noise, which stems mainly from the LNAs (but also from other components) [8], which can be jointly modeled as noisy two-ports. There is an equivalent model [20] for each of the noisy two-ports consisting of a noiseless two-port with a voltage and a current noise source,  $u_{N,m}, i_{N,m}$ , at its input, which model the intrinsic noise. The SNR at the input and the output of the noiseless two-port is the same and thus it is sufficient to only consider the input port in the model [9].

The noise distributions are modeled as [8]

$$\begin{aligned} \mathbf{u}_A &\sim \mathcal{N}_{\mathbb{C}}(\mathbf{0} \text{ V}, \mathbf{R}_A), & \mathbf{R}_A &= 4k_B T_A \Delta f \text{Re}(\mathbf{Z}_{22}), \\ \mathbf{u}_N &\sim \mathcal{N}_{\mathbb{C}}(\mathbf{0} \text{ V}, \sigma_u^2 \mathbf{I}), & \mathbf{i}_N &\sim \mathcal{N}_{\mathbb{C}}(\mathbf{0} \text{ A}, \sigma_i^2 \mathbf{I}) \end{aligned} \quad (6)$$

for some  $\sigma_u > 0 \text{ V}, \sigma_i > 0 \text{ A}$ , where  $k_B$  is the Boltzmann constant,  $\Delta f$  is the noise bandwidth and  $T_A$  is the noise temperature of the antennas. In the noise-free case,

$$\mathbf{u}_L|_{\text{nf}} = \mathbf{u}_2|_{\text{nf}} = \mathbf{Z}_{21} \mathbf{i}_1 + \mathbf{Z}_{22} \mathbf{i}_2|_{\text{nf}} = -\mathbf{Z}_L \mathbf{i}_2|_{\text{nf}}. \quad (7)$$

Combining (3), (4) and (7) leads to

$$\begin{aligned} \mathbf{u}_L|_{\text{nf}} &= \mathbf{D} \mathbf{u}_G, \\ \mathbf{D} &= \mathbf{Z}_L (\mathbf{Z}_{22} + \mathbf{Z}_L \mathbf{I})^{-1} \mathbf{Z}_{21} (\mathbf{Z}_{11} + \mathbf{Z}_G \mathbf{I})^{-1}. \end{aligned} \quad (8)$$

In the signal-free case, the intrinsic noise sources  $\mathbf{u}_N$  and  $\mathbf{i}_N$  are assumed to be uncorrelated with the extrinsic noise  $\mathbf{u}_A$ .  $u_{N,m}$  and  $i_{N,m}$  are correlated with the correlation coefficient [8]

$$\rho = \frac{\text{E}[u_{N,m} i_{N,m}^*]}{\sigma_u \sigma_i} \quad \forall m. \quad (9)$$

Consider the following two equations that follow from Kirchhoff's voltage and current law:

$$-\mathbf{u}_A + \mathbf{u}_N + \mathbf{u}_L|_{\text{sf}} = \mathbf{Z}_{22} \mathbf{i}_2|_{\text{sf}}, \quad (10)$$

$$\mathbf{i}_2|_{\text{sf}} = \mathbf{i}_N - \mathbf{Z}_L^{-1} \mathbf{u}_L|_{\text{sf}}. \quad (11)$$

Eliminating  $\mathbf{i}_2|_{\text{sf}}$  and solving for  $\mathbf{u}_L|_{\text{sf}}$  gives the relation between  $\boldsymbol{\eta}$  and the noise sources

$$\boldsymbol{\eta} = \frac{\mathbf{u}_L|_{\text{sf}}}{\sqrt{R_L}} = \frac{Z_L}{\sqrt{R_L}} (\mathbf{Z}_{22} + \mathbf{Z}_L \mathbf{I})^{-1} (\mathbf{u}_A - \mathbf{u}_N + \mathbf{Z}_{22} \mathbf{i}_N). \quad (12)$$

Together with (6) and (9), the noise covariance matrix can be computed as

$$\begin{aligned} \mathbf{R}_{\boldsymbol{\eta}} &= \text{E}[\boldsymbol{\eta} \boldsymbol{\eta}^H] = \frac{|Z_L|^2}{R_L} (\mathbf{Z}_{22} + \mathbf{Z}_L \mathbf{I})^{-1} \mathbf{Q} (\mathbf{Z}_{22} + \mathbf{Z}_L \mathbf{I})^{-H}, \\ \mathbf{Q} &= \sigma_u^2 \mathbf{I} + \sigma_i^2 \mathbf{Z}_{22} \mathbf{Z}_{22}^* - 2\sigma_u \sigma_i \text{Re}(\rho^* \mathbf{Z}_{22}) + \mathbf{R}_A. \end{aligned} \quad (13)$$

The transmit power in the physical model can be computed as

$$\begin{aligned} P_T &= \text{E}[\text{Re}(i_1^H \mathbf{u}_1)] = \frac{\text{E}[\mathbf{u}_G^H \mathbf{B} \mathbf{u}_G]}{R_G}, & R_G &:= \text{Re}(Z_G), \\ \mathbf{B} &= R_G (\mathbf{Z}_{11} + \mathbf{Z}_G \mathbf{I})^{-H} \text{Re}(\mathbf{Z}_{11}) (\mathbf{Z}_{11} + \mathbf{Z}_G \mathbf{I})^{-1}, \end{aligned} \quad (14)$$

where we have used (3) and where  $\mathbf{B}$  is the so-called power-coupling matrix [8]. Then the complete physical model is

$$\begin{aligned} \mathbf{u}_L &= \mathbf{D} \mathbf{u}_G + \sqrt{R_L} \boldsymbol{\eta}, & \boldsymbol{\eta} &\sim \mathcal{N}_{\mathbb{C}}(\mathbf{0} \sqrt{\mathbf{W}}, \mathbf{R}_{\boldsymbol{\eta}}), \\ P_T &= \frac{\text{E}[\mathbf{u}_G^H \mathbf{B} \mathbf{u}_G]}{R_G}. \end{aligned} \quad (15)$$

### B. Information-Theoretic Model

Consider the typical information-theoretic model (e.g., [21, Ch. 1])

$$\begin{aligned} \mathbf{y} &= \mathbf{H} \mathbf{x} + \boldsymbol{\vartheta}, & \boldsymbol{\vartheta} &\sim \mathcal{N}_{\mathbb{C}}(\mathbf{0} \sqrt{\mathbf{W}}, \sigma_{\boldsymbol{\vartheta}}^2 \mathbf{I}), & \sigma_{\boldsymbol{\vartheta}} &> 0 \sqrt{\mathbf{W}}, \\ P_T &= \text{E}[\mathbf{x}^H \mathbf{x}], \end{aligned} \quad (16)$$

which allows existing techniques and results for capacity and achievable rates to be easily drawn on. In order to get a physically consistent information-theoretic model, we need to ensure that the transmit power  $P_T$  and the noise covariance are consistent with the physical model (15). This can be achieved by a linear mapping from  $\mathbf{u}_G$  and  $\mathbf{u}_L$  to  $\mathbf{x}$  and  $\mathbf{y}$ ,

$$\mathbf{x} = \frac{1}{\sqrt{R_G}} \mathbf{B}^{H/2} \mathbf{u}_G, \quad \text{s.t.} \quad \mathbf{B} = \mathbf{B}^{1/2} \mathbf{B}^{H/2}, \quad (17)$$

$$\mathbf{y} = \frac{\sigma_{\boldsymbol{\vartheta}}}{\sqrt{R_L}} \mathbf{R}_{\boldsymbol{\eta}}^{-1/2} \mathbf{u}_L, \quad (18)$$

as shown in [8], [9] and leads to the system model shown in Fig. 2. Throughout the paper, we assume that matrix square roots in general fulfill a condition similar to (17). The expressions are not exactly the same as in [8], [9], because  $\mathbf{B}^{1/2}$  is not unique and in these two papers, only  $\mathbf{B}^{1/2}$  that are Hermitian are considered. We choose

$$\begin{aligned} \mathbf{B}^{1/2} &= \sqrt{R_G} (\mathbf{Z}_{11} + \mathbf{Z}_G \mathbf{I})^{-H} \text{Re}(\mathbf{Z}_{11})^{1/2}, \\ \text{s.t.} \quad \text{Re}(\mathbf{Z}_{11}) &= \text{Re}(\mathbf{Z}_{11})^{1/2} \text{Re}(\mathbf{Z}_{11})^{1/2}, \end{aligned} \quad (19)$$

$$\mathbf{R}_{\boldsymbol{\eta}}^{1/2} = \frac{Z_L}{\sqrt{R_L}} (\mathbf{Z}_{22} + \mathbf{Z}_L \mathbf{I})^{-1} \mathbf{Q}^{1/2}. \quad (20)$$

This leads to the information-theoretic channel

$$\begin{aligned} \mathbf{H} &= \sigma_{\boldsymbol{\vartheta}} \frac{\sqrt{R_G}}{\sqrt{R_L}} \mathbf{R}_{\boldsymbol{\eta}}^{-1/2} \mathbf{D} \mathbf{B}^{-H/2} \\ &= \sigma_{\boldsymbol{\vartheta}} \mathbf{Q}^{-1/2} \mathbf{Z}_{21} \text{Re}(\mathbf{Z}_{11})^{-1/2}, \end{aligned} \quad (21)$$

which captures the physical context [8], [9].  $\sigma_\vartheta$  is an arbitrary scaling, but to ensure that the sum noise powers in the physical and information-theoretic models are the same, i.e.,

$$\mathbb{E}[\vartheta^H \vartheta] = \mathbb{E}[\eta^H \eta] \quad (22)$$

holds, let

$$\sigma_\vartheta^2 = \frac{\text{tr}(\mathbf{R}_\eta)}{M}. \quad (23)$$

### C. Neglecting the Mutual Coupling

There are three matrices that characterize the information-theoretic channel  $\mathbf{H}$ , namely  $\mathbf{B}$ ,  $\mathbf{D}$  and  $\mathbf{R}_\eta$ . The matrix  $\mathbf{D}$  can be estimated with the help of pilot symbols. Independent of whether the mutual coupling is neglected or not, the estimate related to perfect CSI knowledge is always the same  $\mathbf{D}$ . It is the only matrix of the three that is time-variant due to user mobility. The other two are time-invariant.  $\mathbf{B}$  is a function of  $Z_G$  and  $\mathbf{Z}_{11}$  – or equivalently the scattering parameters – which can be determined by off-line modeling, simulation or measurement of the antenna arrays, including the front/back end of the RF chains. In many publications, mutual coupling is ignored, meaning that  $\mathbf{B}$  and  $\mathbf{R}_\eta$  are assumed to be diagonal or scaled identity matrices (see Section IV). Acquiring  $\mathbf{R}_\eta$  is further discussed in the following section.

## III. RECIPROCITY OF THE INFORMATION-THEORETIC CHANNEL

From now on, we relate the models presented in the previous section to the downlink (Fig. 1). The uplink uses a similar model, but with the impedance matrix  $\mathbf{Z}^T$  and with the noise sources at the base station.  $\mathbf{Z}_{11}$  describes the antennas at the base station and  $\mathbf{Z}_{22}$  those at the mobiles. In the following sections, we will assume that  $Z_G = Z_L$ , as  $Z_G \neq Z_L$  will be compensated due to reciprocity calibration. Then, due to the symmetry between “1” and “2” in (8) and as  $\mathbf{Z}_{21} = \mathbf{Z}_{12}^T$  (see (1)), the noiseless relation between generator and load voltage,  $\mathbf{D}$ , is reciprocal, i.e.,

$$\mathbf{D}_{\text{UL}}^T = \mathbf{D} = Z_L(\mathbf{Z}_{22} + Z_L \mathbf{I})^{-1} \mathbf{Z}_{21} (\mathbf{Z}_{11} + Z_G \mathbf{I})^{-1}. \quad (24)$$

However, there is no such symmetry in (21), but

$$\begin{aligned} \mathbf{H} &= \sigma_\vartheta \mathbf{R}_\eta^{-1/2} \mathbf{D} \mathbf{B}^{-H/2} \\ &= \sigma_\vartheta \mathbf{Q}^{-1/2} \mathbf{Z}_{21} \text{Re}(\mathbf{Z}_{11})^{-1/2} \end{aligned} \quad (25)$$

and

$$\begin{aligned} \mathbf{H}_{\text{UL}} &= \sigma_{\vartheta, \text{UL}} \mathbf{R}_{\eta, \text{UL}}^{-1/2} \mathbf{D}_{\text{UL}} \mathbf{B}_{\text{UL}}^{-H/2} \\ &= \sigma_{\vartheta, \text{UL}} \mathbf{Q}_{\text{UL}}^{-1/2} \mathbf{Z}_{12} \text{Re}(\mathbf{Z}_{22})^{-1/2} \end{aligned} \quad (26)$$

hold, so the information-theoretic downlink and uplink channels are not reciprocal in the ordinary way, i.e.,  $\mathbf{H}_{\text{UL}}^T \neq \mathbf{H}$ . Although  $\mathbf{D}$  is reciprocal, in general, a different reciprocity relation is introduced by whitening the noise coupling between the antennas and by maintaining the physical consistency of the transmit power, see (17) and (18). This physically consistent reciprocity relation

$$\mathbf{H} = \frac{\sigma_\vartheta}{\sigma_{\vartheta, \text{UL}}} \mathbf{R}_\eta^{-1/2} \mathbf{B}_{\text{UL}}^{*/2} \mathbf{H}_{\text{UL}}^T \mathbf{R}_{\eta, \text{UL}}^{T/2} \mathbf{B}^{-H/2} \quad (27)$$

is obtained by comparing (25) and (26). If the base station wants to reuse the CSI estimated in the uplink for the downlink, it needs to use this physically consistent reciprocity relation for the information-theoretic channel.

Consider that the base station acquires CSI in the uplink by estimating  $\mathbf{D}_{\text{UL}}$  – instead of  $\mathbf{H}_{\text{UL}}$  – from the mobile(s)’ pilot symbols. To make the downlink physically consistent at the base station, i.e., to apply (17), it needs to know  $\mathbf{B}^{-H/2}$ , anyway, so that it can compute  $\mathbf{D}_{\text{UL}}^T \mathbf{B}^{-H/2}$  without any further information, although compared to (25), there remains the unknown factor  $\sigma_\vartheta \mathbf{R}_\eta^{-1/2}$ .

Let us simplify the model for the MU-MISO downlink and uplink, i.e., when each mobile has a single antenna. We assume that the distance between different mobiles is large with respect to the wavelength. For large distances, the coupling reduces inversely with the distance [9], so it goes to zero and  $\mathbf{Z}_{22}$  becomes diagonal. Furthermore, we assume identical antenna impedances  $Z_A$  at the mobiles, i.e.,

$$\mathbf{Z}_{22} = Z_A \mathbf{I}. \quad (28)$$

Then the downlink information-theoretic channel simplifies to

$$\begin{aligned} \mathbf{R}_\eta &= \sigma_\eta^2 \mathbf{I}, \quad \sigma_\eta^2 = \frac{|Z_L|^2}{R_L |Z_A + Z_L|^2} \sigma_q^2, \quad \mathbf{Q} = \sigma_q^2 \mathbf{I}, \\ \mathbf{H} &= \mathbf{D}_{\text{UL}}^T \mathbf{B}^{-H/2}, \end{aligned} \quad (29)$$

i.e., due to (23), there is no unknown factor  $\sigma_\vartheta \mathbf{R}_\eta^{-1/2}$  in this scenario. The uplink information-theoretic channel simplifies to

$$\mathbf{H}_{\text{UL}} = \sigma_{\vartheta, \text{UL}} \mathbf{R}_{\eta, \text{UL}}^{-1/2} \mathbf{D}_{\text{UL}} \frac{Z_A + Z_G}{\sqrt{R_G \text{Re}(Z_A)}}. \quad (30)$$

Also in this case,  $\mathbf{H}$  and  $\mathbf{H}_{\text{UL}}$  are not reciprocal in the ordinary way.

Note that if the mobiles have more than one antenna, i.e., in MU-MIMO systems,  $\mathbf{Z}_{22}$ ,  $\mathbf{Q}$ ,  $\mathbf{R}_\eta$  and  $\mathbf{B}_{\text{UL}}$  are block diagonal, since we assume that there is no coupling between different mobiles. The noise covariance of multi-antenna mobiles is also a matrix instead of a scalar. Therefore, even if (23) is taken into account,  $\mathbf{D}_{\text{UL}}^T \mathbf{B}^{-H/2} \neq \mathbf{H}$  in general. One solution in practice might be to create a database of noise covariance matrices corresponding to different models of mobiles for the base station. As in conventionally modeled systems, the base station needs feedback from the mobiles about their SNR and needs to deal with  $\mathbf{R}_\eta$ , which is not known perfectly.

## IV. CAPACITIES AND RATES NOT TAKING THE PHYSICAL RECIPROCITY OR THE MUTUAL COUPLING INTO ACCOUNT

In this section, we will compute the ergodic (sum) capacity in the downlink  $C_{\text{erg}}$  and the ergodic (sum) rates when using the ordinary reciprocity relation, instead of the physically consistent one ( $R_{\text{erg, recip}}$ ) and when the base station ignores the coupling at the base station and at the mobiles ( $R_{\text{erg, hyp}}$ ). In particular, we compute the (sum) capacity and rate for a given channel and the ergodic ones are obtained by taking the expectation w.r.t. the channel, i.e., for the (sum) capacity

$$C_{\text{erg}}(P) = \mathbb{E}_{\mathbf{H}}[C(P)], \quad (31)$$

TABLE I  
OVERVIEW OF THE TRANSMIT STRATEGIES

	“cap”	“recip”	“hyp”
Rates	$C, R_{\text{lin}}$	$R_{\text{recip}}, R_{\text{recip,lin}}$	$R_{\text{hyp}}, R_{\text{hyp,lin}}$
Motivation	Capacity achieving strategy.	Naive use of the Multiport Communication Theory.	Conventionally modeled systems.
Description	The base station uses the information-theoretic model (16), as it leads to an easy to use channel model [9], <b>and uses the physically consistent reciprocity relation (27).</b>	The base station uses the information-theoretic model (16), as it leads to an easy to use channel model [9], <b>but assumes that the ordinary reciprocity relation holds.</b>	The base station uses the information-theoretic model ignoring the mutual coupling (see (38), (43), (45) and (53)) and the ordinary reciprocity relation.
Procedure	1: Estimate $\mathbf{D}_{\text{UL}}$ . 2: Compute $\mathbf{H}$ using (26) and (27) (or (29)). 3: Apply the optimal transmit strategy based on $\mathbf{H}$ and $P = P_{\text{T}}$ .	1: Estimate $\mathbf{D}_{\text{UL}}$ . 2: Compute $\mathbf{H}_{\text{UL}}$ using (26). 3: Apply the optimal transmit strategy based on $\mathbf{H}_{\text{UL}}^T$ (corresponding to $\mathbf{h}_{\text{UL}}^*$ for SU-MISO) and $P = P_{\text{T}}$ .	1: Estimate $\mathbf{D}_{\text{UL}}$ . 2: Compute $\hat{\mathbf{H}}$ using (24) and (45). 3: Apply the optimal transmit strategy based on $\hat{\mathbf{H}}'$ (see (55)) and $P = P_{\text{T,p}}$ .
Channel that is transmitted over in the downlink	$\mathbf{H}$	$\mathbf{H}$	$\hat{\mathbf{H}}$

and in a similar way for the (sum) rates. An overview of the different transmit strategies is given in Table I. We assume that the base station obtains an error-free estimate of  $\mathbf{D}_{\text{UL}}$  via pilot symbols and that  $\mathbf{x} \sim \mathcal{N}_{\mathbb{C}}(\mathbf{0}, \sqrt{W}, \mathbf{R}_x)$  with some covariance matrix  $\mathbf{R}_x$ .

#### A. SU-MISO

For a single user, the channel matrices become vectors. Let

$$\mathbf{h} = \mathbf{H}^T, \quad \mathbf{h}_{\text{UL}} = \mathbf{H}_{\text{UL}}, \quad \mathbf{d}_{\text{UL}} = \mathbf{D}_{\text{UL}}. \quad (32)$$

The capacity of the downlink with power  $P$  is [22]

$$C(P) = \log_2 \left( 1 + \frac{P}{\sigma_g^2} \|\mathbf{h}\|_2^2 \right) \text{ for } P_{\text{T}} = P. \quad (33)$$

Let

$$\mathbf{x} = \mathbf{f}s, \quad s \sim \mathcal{N}_{\mathbb{C}}(0, \sqrt{W}, P). \quad (34)$$

Capacity can be achieved by applying the linear precoder

$$\mathbf{f} = \frac{\mathbf{h}^*}{\|\mathbf{h}\|_2}. \quad (35)$$

As  $\mathbf{f}$  can be computed from  $\mathbf{h}$ , which in turn is computed from  $\mathbf{d}_{\text{UL}}$  via (29), estimating  $\mathbf{d}_{\text{UL}}$  in the uplink and using the physically consistent reciprocity relation (27) achieves capacity.

Now consider what happens if the base station uses the information-theoretic model in the up- and downlink, but assumes that the ordinary reciprocity relation  $\mathbf{H} = \mathbf{H}_{\text{UL}}^T$  holds, corresponding to  $\mathbf{h} = \mathbf{h}_{\text{UL}}$  for SU-MISO. This means it determines the information-theoretic uplink channel  $\mathbf{h}_{\text{UL}}$  via (26), and then chooses the optimal precoder based on  $\mathbf{h}_{\text{UL}}^*$ ,

$$\mathbf{f}_{\text{recip}} = \frac{\mathbf{h}_{\text{UL}}^*}{\|\mathbf{h}_{\text{UL}}\|_2} \quad (36)$$

leading to the rate

$$R_{\text{recip}}(P) = \log_2 \left( 1 + \frac{P}{\sigma_g^2} \frac{|\mathbf{h}^H \mathbf{h}_{\text{UL}}^*|^2}{\|\mathbf{h}_{\text{UL}}\|_2^2} \right) \text{ for } P_{\text{T}} = P. \quad (37)$$

Note that this rate is different from (33) and there will be some rate loss compared to capacity.

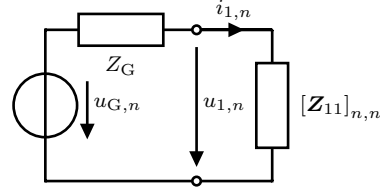


Fig. 3. Simplified circuit for measuring  $P_{\text{T},n}$ .

For comparison, let us also consider what happens if the base station ignores the coupling. This means that it does not use Multiport Communication Theory, but rather conventional modeling. To predict how much power the base station radiates, it needs to know the power coupling matrix  $\hat{\mathbf{B}}$  that ignores the mutual coupling and uses the mapping

$$\hat{\mathbf{x}} = \frac{1}{\sqrt{R_G}} \hat{\mathbf{B}}^{H/2} \mathbf{u}_G. \quad (38)$$

$\hat{\mathbf{B}}$  is diagonal and its diagonal entries can be obtained by connecting a linear generator to only one antenna in the array at a time, terminating the other antennas with open circuits and measuring the power  $P_{\text{T,p},n}$  flowing into the antenna. This means that when the  $n$ th antenna is excited with the voltage  $u_{G,n}$  corresponding to some  $\hat{x}_n, i_{1,n'} = 0 \text{ A } \forall n' \neq n$  and the relevant part of the circuit reduces to a simple voltage divider (Fig. 3). The base station predicts that it radiates

$$P_{\text{T,p},n} = |u_{G,n}|^2 \frac{\text{Re}([\mathbf{Z}_{11}]_{n,n})}{|[\mathbf{Z}_{11}]_{n,n} + Z_G|^2}. \quad (39)$$

Similar to (15), we also have

$$P_{\text{T,p},n} = |u_{G,n}|^2 \frac{[\hat{\mathbf{B}}]_{n,n}}{R_G}. \quad (40)$$

Thus analogously to (14),  $\hat{\mathbf{B}}$  is given by

$$\hat{\mathbf{B}} = R_G (\text{diag}(\mathbf{Z}_{11}) + Z_G \mathbf{I})^{-H} \text{Re}(\text{diag}(\mathbf{Z}_{11})) \cdot (\text{diag}(\mathbf{Z}_{11}) + Z_G \mathbf{I})^{-1} \quad (41)$$

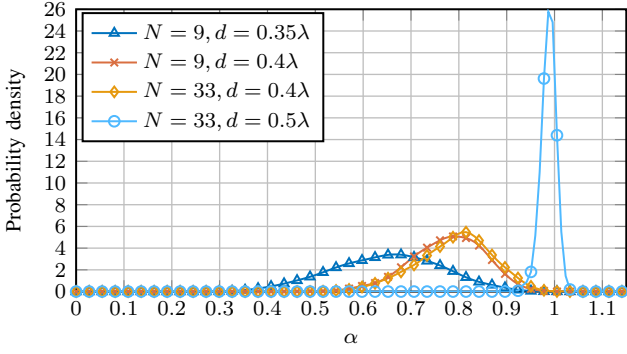


Fig. 4. Probability density of  $\alpha$  for a uniform circular array (UCA) for four scenarios in a SU-MISO i.i.d. channel.

and

$$\hat{\mathbf{B}}^{1/2} = \sqrt{R_G}(\text{diag}(\mathbf{Z}_{11}) + Z_G \mathbf{I})^{-H} \text{Re}(\text{diag}(\mathbf{Z}_{11}))^{1/2}. \quad (42)$$

If the impedance of all base station antennas is the same, i.e.,  $\text{diag}(\mathbf{Z}_{11})$  is a scaled identity matrix, then  $\hat{\mathbf{B}}$  is also a scaled identity matrix. For an arbitrary excitation of the antenna array, the base station predicts the radiated power as [22]

$$P_{T,p} = \text{E}[\|\hat{\mathbf{x}}\|_2^2] = \frac{\text{E}[\mathbf{u}_G^H \hat{\mathbf{B}} \mathbf{u}_G]}{R_G}. \quad (43)$$

As  $\mathbf{x}$  is a zero-mean Gaussian random variable and as

$$\hat{\mathbf{x}} = \mathbf{B}^{-H/2} \hat{\mathbf{B}}^{H/2} \mathbf{x}, \quad (44)$$

$\hat{\mathbf{x}} \sim \mathcal{N}_C(\mathbf{0}, \sqrt{\mathbf{W}}, \mathbf{R}_x)$ . Due to the mapping (38), the base station does not transmit over the information-theoretic channel  $\mathbf{H}$ , but over another information-theoretic channel  $\hat{\mathbf{H}}$ , the one ignoring the coupling, as given by [22]

$$\hat{\mathbf{H}} = \sigma_\vartheta \mathbf{R}_\eta^{-1/2} \mathbf{D} \hat{\mathbf{B}}^{-H/2}. \quad (45)$$

For SU-MISO, let  $\mathbf{d} = \mathbf{D}^T$  so that we can define the column vector

$$\hat{\mathbf{h}}^T = \hat{\mathbf{H}} \stackrel{(23)}{=} \mathbf{d}^T \hat{\mathbf{B}}^{-H/2}. \quad (46)$$

When the base station uses a precoder similar to (35),

$$\mathbf{f}_{\text{hyp}} = \frac{\hat{\mathbf{h}}^*}{\|\hat{\mathbf{h}}\|_2}, \quad (47)$$

it can achieve the (hypothetical) rate [22]

$$R_{\text{hyp}}(P) = \log_2 \left( 1 + \frac{P}{\sigma_\vartheta^2} \|\hat{\mathbf{h}}\|_2^2 \right) \text{ for } P_{T,p} = P. \quad (48)$$

We call the rate hypothetical because it is what the base station assumes to achieve. However when base station predicts that it radiates the power  $P_{T,p} = P$  and uses  $\mathbf{f}_{\text{hyp}}$ , its (true) radiated power  $P_T \neq P$  in general. Consider the ratio  $\alpha$  [22] that follows from (15), (43), (44) and (47),

$$\alpha = \frac{P_T}{P_{T,p}} = \frac{\hat{\mathbf{h}}^*}{\|\hat{\mathbf{h}}\|_2} \hat{\mathbf{B}}^{-1/2} \mathbf{B} \hat{\mathbf{B}}^{-H/2} \frac{\hat{\mathbf{h}}^T}{\|\hat{\mathbf{h}}\|_2}. \quad (49)$$

$\alpha$  is a function of the channel and for some of its realizations,

$$\alpha < 1 \Leftrightarrow P_{T,p} > P_T \quad \text{or} \quad \alpha > 1 \Leftrightarrow P_{T,p} < P_T, \quad (50)$$

see Figs. 4 and 17, but  $P_{T,p} < P_T$  is extremely rare for  $d = 0.35\lambda$  and  $d = 0.4\lambda$ , but less so for  $d = 0.5\lambda$ . Therefore, depending on the channel realization, there will be rate curves that actually require more or less transmit power than predicted. On the one hand, if  $\alpha > 1$  and if  $P_{T,p}$  is as large as the power available linearly from the power amplifiers, there will be non-linear distortions due to  $P_T > P_{T,p}$ , which may cause transmission failure. On the other hand, if  $\alpha < 1$ , i.e.,  $P_T < P_{T,p}$ , the transmission will be successful but the power budget is not fully utilized.

The probability densities in this paper are estimated on a grid of 128 points in a Monte Carlo simulation (see Sections V and VI) using the MATLAB implementation [23] based on the theory in [24] with a Gaussian kernel. Note that  $\alpha$  does not need to be estimated in the communication system; it is only introduced to explain the simulation results.

## B. SU-MIMO

For SU-MIMO, the capacity in the downlink with power  $P$  is given by [25]

$$C(P) = \log_2 |\mathbf{I} + \sigma_\vartheta^{-2} \mathbf{H}^H \mathbf{H} \mathbf{R}_x| \text{ for } P_T = P, \quad (51)$$

$$\mathbf{R}_x = \mathbf{V} \Psi \mathbf{V}^H, \quad \text{tr}(\Psi) = P,$$

where  $\mathbf{V}$  is obtained from the eigenvalue decomposition (EVD)

$$\mathbf{H}^H \mathbf{H} = \mathbf{V} \Phi \mathbf{V}^H \quad (52)$$

and  $\Psi$  is a diagonal matrix whose entries are determined via waterfilling. This can be achieved by transmitting  $\mathbf{s} \sim \mathcal{N}_C(\mathbf{0}, \sqrt{\mathbf{W}}, \Psi)$  over the precoder  $\mathbf{V}$ , i.e.,  $\mathbf{x} = \mathbf{V} \mathbf{s}$ .

If the base station ignores the mutual coupling at the base station and at the mobiles, it uses (38) to transform from  $\hat{\mathbf{x}}$  to  $\mathbf{u}_G$  as in SU-MISO, assumes that mobile uses the mapping

$$\hat{\mathbf{y}} = \frac{\sigma_\vartheta}{\sqrt{R_L}} \hat{\mathbf{R}}_\eta^{-1/2} \mathbf{u}_L, \quad \hat{\mathbf{R}}_\eta = \text{diag}(\mathbf{R}_\eta) \quad (53)$$

instead of (18), and assumes that

$$\hat{\vartheta} \sim \mathcal{N}_C(\mathbf{0}, \sqrt{\mathbf{W}}, \sigma_\vartheta^2 \mathbf{I}) \quad (54)$$

holds. Similar to (51), the optimal transmit strategy is to choose the precoder  $\hat{\mathbf{V}}'$  from the singular value decomposition (SVD) of the channel

$$\hat{\mathbf{H}}' = \sigma_\vartheta \hat{\mathbf{R}}_\eta^{-1/2} \mathbf{D} \hat{\mathbf{B}}^{-H/2} = \hat{\mathbf{U}}' \hat{\Phi}'^{1/2} \hat{\mathbf{V}}'^H \quad (55)$$

and the corresponding diagonal power allocation matrix  $\hat{\Psi}'$  obtained by waterfilling.

However, the noise distribution at the mobile in the information-theoretic model is

$$\hat{\vartheta} \sim \mathcal{N}_C(\mathbf{0}, \sqrt{\mathbf{W}}, \hat{\mathbf{R}}_\vartheta), \quad (56)$$

$$\hat{\mathbf{R}}_\vartheta = \sigma_\vartheta^2 \hat{\mathbf{R}}_\eta^{-1/2} \mathbf{R}_\eta \hat{\mathbf{R}}_\eta^{-H/2},$$

contrary to what the base station expects, see (54). Only  $\text{diag}(\hat{\mathbf{R}}_\vartheta) = \sigma_\vartheta^2 \mathbf{I}$  holds. This leads to the (hypothetical) rate

$$R_{\text{hyp}}(P) = \log_2 |\mathbf{I} + \sigma_\vartheta^{-2} \hat{\mathbf{H}}^H \hat{\mathbf{H}} \mathbf{R}_x| \text{ for } P_{T,p} = P, \quad (57)$$

$$\mathbf{R}_x = \hat{\mathbf{V}}' \hat{\Psi}' \hat{\mathbf{V}}'^H, \quad \text{tr}(\hat{\Psi}') = P.$$

Similar to (48), this is only a hypothetical rate, since the true radiated power may be different from the predicted one. By generalization of (49), we consider the ratio

$$\alpha(P) := \frac{P_T}{P_{T,p}} = \frac{\text{tr}(\hat{\mathbf{B}}^{-1/2} \mathbf{B} \hat{\mathbf{B}}^{-H/2} \mathbf{R}_{\hat{x}})}{P} = \text{tr}(\mathbf{A}(P)),$$

$$\mathbf{A}(P) = \hat{\mathbf{B}}^{-1/2} \mathbf{B} \hat{\mathbf{B}}^{-H/2} \hat{\mathbf{V}}' \frac{\hat{\Psi}}{P} \hat{\mathbf{V}}'^{H}. \quad (58)$$

Contrary to SU-MISO, for SU-MIMO  $\alpha$  also depends on the power allocation.

When the base station uses the ordinary reciprocity relation instead of the physically consistent one, the optimal transmit strategy is to use the precoder  $\mathbf{V}_{\text{recip}}$  from the EVD

$$\mathbf{H}_{\text{UL}}^* \mathbf{H}_{\text{UL}}^T = \mathbf{V}_{\text{recip}} \Phi_{\text{recip}} \mathbf{V}_{\text{recip}}^H, \quad (59)$$

and  $\Psi_{\text{recip}}$  determined via waterfilling. The rate of this scheme is

$$R_{\text{recip}}(P) = \log_2 |\mathbf{I} + \sigma_{\vartheta}^{-2} \mathbf{R}_x \mathbf{H}^H \mathbf{H}| \text{ for } P_T = P,$$

$$\mathbf{R}_x = \mathbf{V}_{\text{recip}} \Psi_{\text{recip}} \mathbf{V}_{\text{recip}}^H, \quad \text{tr}(\Psi_{\text{recip}}) = P. \quad (60)$$

### C. MU-MISO and MU-MIMO

The sum capacity of the MU-MISO/MIMO Broadcast channel (BC) is given by [26], [27]

$$C(P) = \max_{\substack{\Xi \succeq \mathbf{0} \\ \text{tr}(\Xi) \leq P}} \log_2 |\mathbf{I} + \sigma_{\vartheta}^{-2} \mathbf{H}^H \Xi \mathbf{H}| \text{ for } P_T = P, \quad (61)$$

where  $\Xi$  is the (block-)diagonal covariance matrix in the dual Multiple Access Channel (MAC), i.e., it is based on the rate duality between the BC and the dual MAC with the channel  $\mathbf{H}^H$ . For MU-MIMO, we use the duality from [28], which ensures that streams allocated to the same mobile are orthogonal. Equation (61) describes a convex optimization problem that can be solved efficiently by various optimization algorithms, e.g., a projected gradient algorithm [29] with a step-size control as in [30, eq. (14)].

For MU-MISO, if the base station ignores the mutual coupling at the base station, it will perform an optimization as in (61), namely

$$R_{\text{hyp}}(P) = \max_{\substack{\hat{\Xi} \succeq \mathbf{0} \\ \text{tr}(\hat{\Xi}) \leq P}} \log_2 |\mathbf{I} + \sigma_{\vartheta}^{-2} \hat{\mathbf{H}}^H \hat{\Xi} \hat{\mathbf{H}}| \text{ for } P_{T,p} = P. \quad (62)$$

Note that this only holds as mutual coupling at the base station does not introduce interference, no matter whether taken into account or not – as long as the base station has got perfect channel knowledge.

For MU-MIMO, when the base station ignores the mutual coupling at the base station and at the mobiles, or when it uses the ordinary reciprocity relation in the information-theoretic model, the analysis is more involved, since the channel the base station expects and the true channel are different. This is similar to a channel estimation error and this leads to interference. The capacity achieving transmission scheme for perfect channel knowledge is Dirty Paper Coding (DPC). When this scheme is used with a channel estimation error, the achievable rate may even be lower than with linear precoding. This is shown for a lattice-based scheme in a two-user MU-MISO BC in [31].

When computing the achievable sum rate with linear precoding, a global optimization is required as this problem is non-convex, see e.g., [32], [33], which optimizes over the transmit covariance in the dual MAC globally. This is only feasible for a small number of users and their antennas. Instead, we use a linear zero forcing (ZF) approach for the comparison that is only guaranteed to find a local optimum. Among several algorithms in the literature [34], [35], we have chosen LISA [34], which is an elegant greedy weighted sum rate maximization algorithm with low complexity and very good performance. For the comparison we are considering, the choice of the weighted sum rate maximization algorithm is not substantial. LISA finds the ZF precoder and power allocation, where we use the variant that does not avoid the matrix inversion to optimize the receive filters. Applying it to  $\mathbf{H}$ ,  $\hat{\mathbf{H}}'$  and  $\mathbf{H}_{\text{UL}}^T$  for  $P_T = P$ ,  $P_{T,p} = P$  and  $P_T = P$  and transmitting over  $\mathbf{H}$ ,  $\hat{\mathbf{H}}$  and  $\mathbf{H}$  respectively, leads to  $R_{\text{lin}}$ ,  $R_{\text{hyp,lin}}$  and  $R_{\text{recip,lin}}$ . When computing the rates, we do not consider the equalizers at the mobiles, in other words, we assume that they employ an optimum equalization.

## V. SIMULATIONS FOR THE I.I.D. CHANNELS

In the following, we assume a base station with a uniform circular array (UCA) of  $N$  parallel infinitely thin, but perfectly conducting  $\lambda/2$ -dipoles with antenna spacing  $d$ , and one or more mobiles with a UCA consisting also of parallel  $\lambda/2$ -dipoles. Their impedance matrices can be obtained in a similar way as for  $\lambda/4$ -monopoles as shown in [18] (which is based on [19, Ch. 13]), as they are canonical minimum scattering antennas [36], [37]. Let  $Z_A$  be the self-impedance of the  $\lambda/2$ -dipoles. We assume the heuristic match  $Z_G = Z_L = \text{Re}(Z_A)$  [22], which matches the real part of the antenna impedance to the purely resistive source and load impedance.  $\mathbf{Q}^{1/2}$  is obtained by the (lower triangular) Cholesky decomposition of  $\mathbf{Q}$ .

For the noise parameters, we use the measured ones from [38, Tables IV & VI] with a noise bandwidth of 740 kHz, except that we assume  $\text{Re}(Z_A)$  as the input impedance of the LNA, so it fits our model. In this section we also assume that the entries of  $\mathbf{Z}_{21}$  are i.i.d. according to  $\mathcal{N}_{\mathbb{C}}(0, \Omega, \sigma_z^2)$ . In order to obtain reasonable transmit powers,  $\sigma_z \approx 0.019085 \Omega$  is chosen, which corresponds to the absolute value of the mutual impedance between two  $\lambda/2$ -dipoles separated by  $1000\lambda$ , which is about 85.7 m at 3.5 GHz.

The ergodic (sum) capacity and rates, the average number of active streams and the empirical probability density of  $\alpha$  in the following were computed by a Monte Carlo simulation with 1000 channel realizations.

### A. SU-MISO

Consider one single antenna receiver in four scenarios: a base station with  $N = 9$  antennas and  $d = 0.35\lambda$  or  $d = 0.4\lambda$  antenna spacing and one with  $N = 33$  and  $d = 0.4\lambda$  or  $d = 0.5\lambda$ . Fig. 4 shows the probability density for  $\alpha$  in these scenarios. The largest variation in  $\alpha$  is obtained for a small antenna spacing of  $0.35\lambda$ , where for some channel realizations only about 36.2% of the predicted power is radiated and for some as much as 94.0%. The variations for  $0.4\lambda$  antenna spacing are less pronounced, but there is still a considerable

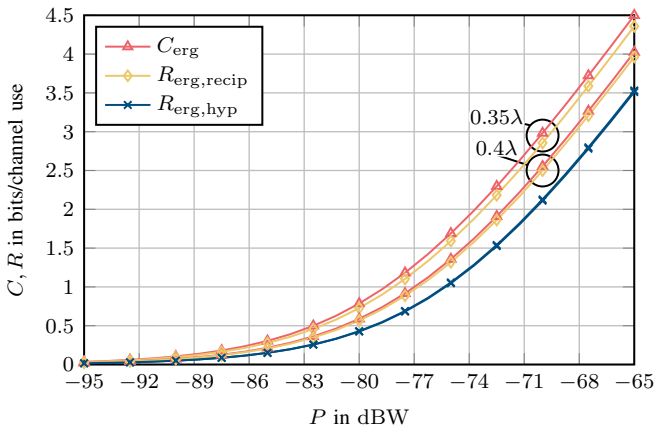


Fig. 5. Ergodic downlink rates for a UCA with 9  $\lambda/2$ -dipoles, and  $0.35\lambda$  and  $0.4\lambda$  antenna spacing in a SU-MISO i.i.d. channel (based on [16]).

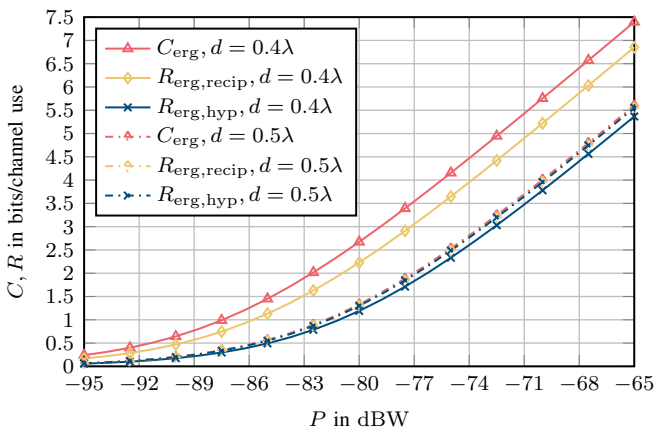


Fig. 6. Ergodic downlink rates for a UCA with 33  $\lambda/2$ -dipoles, and  $0.4\lambda$  and  $0.5\lambda$  antenna spacing in a SU-MISO i.i.d. channel (based on [16]).

variation in  $\alpha$ . For  $d = 0.5\lambda$  there is even less variation. Furthermore, there is a trend that the larger  $d$  is, the further the mass of the distribution of  $\alpha$  moves to larger values of  $\alpha$ . We conclude that the base station radiates on average less power than predicted when it uses conventional modeling. The loss in power is significantly larger for  $d = 0.35\lambda$  than for  $d = 0.4\lambda$ , and in turn than for  $d = 0.5\lambda$ .

Figs. 5 and 6 show the ergodic capacities and rates for these scenarios. Comparing them, we can see that for the same  $P$ ,  $C_{\text{erg}}$  and  $R_{\text{erg,recip}}$  are larger for  $N = 33$  than for  $N = 9$ , and larger for smaller  $d$  than for larger  $d$ . Therefore, a smaller  $d$  is advantageous.  $R_{\text{erg,hyp}}$  only changes very little from  $d = 0.35\lambda$  to  $0.4\lambda$ , and increases slightly from  $d = 0.4\lambda$  to  $0.5\lambda$ . We can also see that using the ordinary reciprocity relation in the information-theoretic model leads to a loss in rate that is small for larger antenna spacings and a small number of antennas, but increases considerably for smaller antenna spacings and a large number of antennas. This loss is caused by the precoder  $\mathbf{f}_{\text{recip}}$ , leading to the beamforming vector  $\sqrt{R_G} \mathbf{B}^{-H/2} \mathbf{f}_{\text{recip}}$ . Both are optimal for the ordinary reciprocity relation, but not for the physically consistent one. Still, using the ordinary reciprocity relation is considerably better than using conventional modeling.  $R_{\text{erg,hyp}}$  shows the

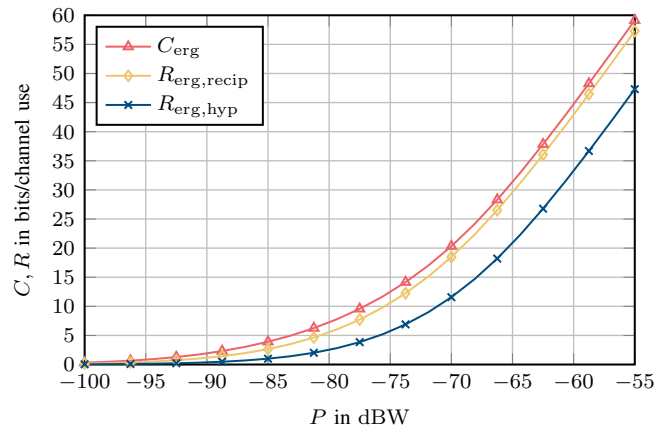


Fig. 7. Ergodic downlink rates for a UCA with 33  $\lambda/2$ -dipoles at the base station and a mobile with a UCA with 9  $\lambda/2$ -dipoles, both with  $0.4\lambda$  antenna spacing, in a SU-MIMO i.i.d. channel.

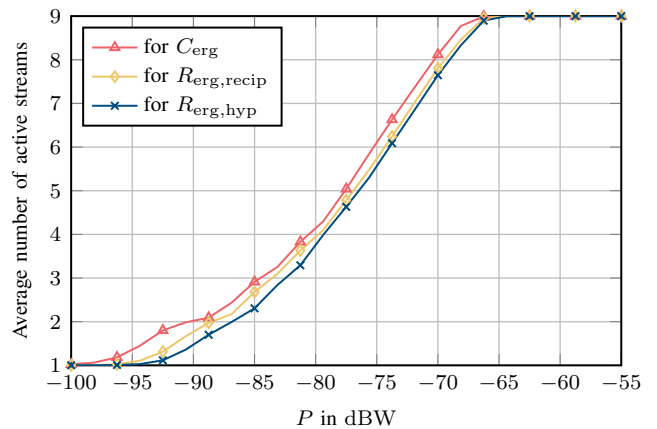


Fig. 8. Average number of active streams for a UCA with 33  $\lambda/2$ -dipoles at the base station and a mobile with a UCA with 9  $\lambda/2$ -dipoles, both with  $0.4\lambda$  antenna spacing, in a SU-MIMO i.i.d. channel.

same tendency as  $R_{\text{erg,recip}}$ , but the gap to  $C_{\text{erg}}$  is significantly larger than for  $R_{\text{erg,recip}}$ . This gap is not only caused by a suboptimal precoder, but also by the base station not being able to accurately predict the radiated power  $P_T$  with conventional modeling. Note that mutual coupling is present independent of the antenna separation and does not decrease monotonically with increasing  $d$ , but rather follows a more complicated relation. It decreases monotonically approximately between  $d = 0$  and  $\lambda/2$ , though. If we increase the number of base station antennas further, e.g., to  $N = 65$ , we see that the trends going from  $N = 9$  to 33 continue.

## B. SU-MIMO

Consider a base station with a UCA consisting of  $N = 33$   $\lambda/2$ -dipoles and a mobile with a UCA with  $M = 9$   $\lambda/2$ -dipoles, both with  $0.4\lambda$  antenna spacing. Compared to SU-MISO (see Fig. 6), the difference between  $R_{\text{erg,hyp}}$  and  $C_{\text{erg}}$  is significantly larger, as shown in Fig. 7, although the antenna spacing at the base station is the same. As in SU-MISO,  $R_{\text{erg,recip}}$  achieves a better performance than  $R_{\text{erg,hyp}}$ .

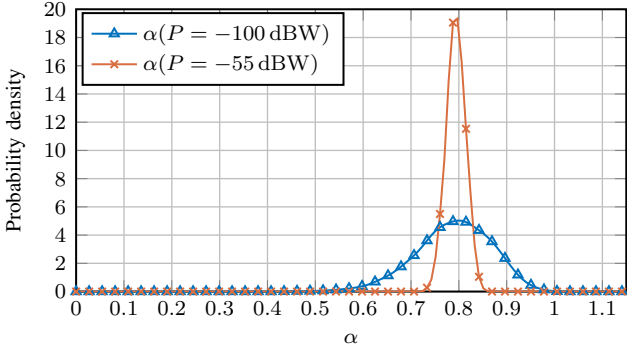


Fig. 9. Probability density of  $\alpha$  for a UCA with  $33 \lambda/2$ -dipoles at the base station and a mobile with a UCA with  $9 \lambda/2$ -dipoles, both with  $0.4\lambda$  antenna spacing, in a SU-MIMO i.i.d. channel.

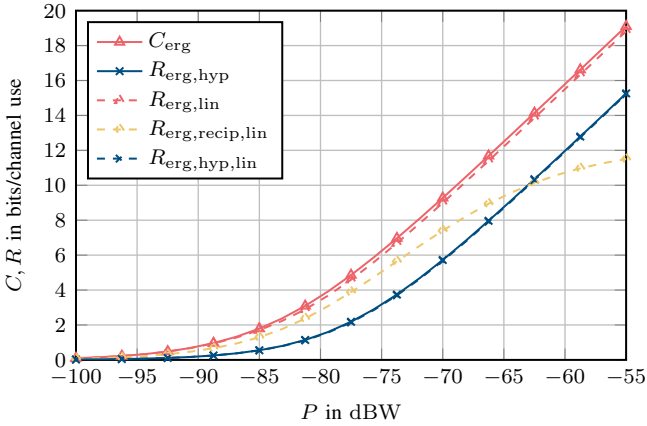


Fig. 10. Ergodic downlink sum rates for a UCA with  $33 \lambda/2$ -dipoles with  $0.4\lambda$  antenna spacing at the base station and two mobiles in a MU-MISO i.i.d. channel.

Looking at the average number of active streams (Fig. 8), all schemes perform similarly. This means the rate difference comes mainly from radiating a different amount of power than predicted and from the suboptimal precoders, instead of a suboptimal number of active streams.

Regarding the predicted radiated power  $P_{T,p}$  when ignoring the coupling, consider the probability density of  $\alpha$  in Fig. 9. For  $P = -100$  dBW, the average number of active streams is 1, and the distribution is similar to Fig. 4. However for  $P = -55$  dBW, the average number of active streams is close to 9, and the distribution is much more narrow around  $\alpha \approx 0.79$ . This means that when more streams are active, there is an averaging effect between streams belonging to directions with large  $\alpha$  and to those with small  $\alpha$ . Note that the ratio of the predicted to the radiated power of the individual streams may still experience a distribution similar to when only one stream is active.

### C. MU-MISO

Let us compare the ergodic sum rates in Fig. 10 for a base station with  $N = 33 \lambda/2$ -dipoles in a UCA communicating to two mobiles with one  $\lambda/2$ -dipole each. The performance of linear ZF precoding is very close to DPC for both, the sum

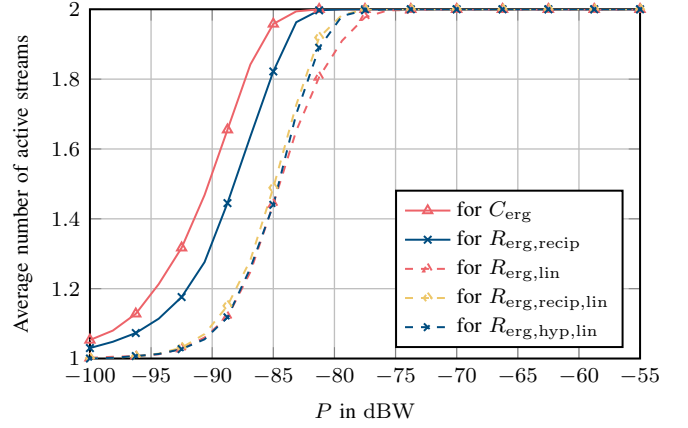


Fig. 11. Average number of active streams for a UCA with  $33 \lambda/2$ -dipoles with  $0.4\lambda$  antenna spacing at the base station and two mobiles in a MU-MISO i.i.d. channel.

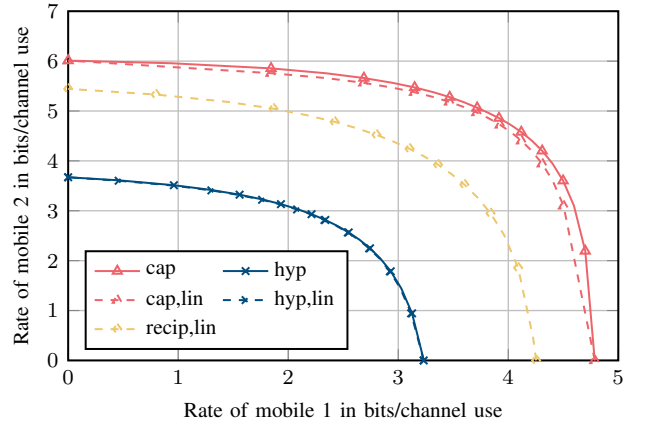


Fig. 12. Rate region for one channel realization for a UCA with  $33 \lambda/2$ -dipoles with  $0.4\lambda$  antenna spacing at the base station and two mobiles in a MU-MISO i.i.d. channel for  $P = -70.57$  dBW.

capacity and the hypothetical sum rate, although fewer streams are active with linear precoding up to around  $P = -75$  dBW, see Fig. 11. The loss when ignoring the coupling ( $R_{\text{erg,hyp}}$ ) is qualitatively similar to the loss for SU-MIMO in Fig. 7. For  $R_{\text{erg,recip,lin}}$ , the loss is smaller than for  $R_{\text{erg,hyp,lin}}$  for small transmit powers – and as shown in Fig. 11, there is only a bit more than one stream active on average. This means that in this region, the system behaves similarly to a SU-MISO system and is mainly noise limited. For larger transmit powers, however, the loss starts to increase significantly when 2 streams are active on average, because using the ordinary reciprocity relation leads to wrong CSI in the downlink and causes interference. The larger this interference is compared to the noise power, the more important it is. For large interference, the system becomes interference limited and  $R_{\text{erg,recip,lin}}$  saturates. This is why starting from  $P \approx -63$  dBW,  $R_{\text{erg,recip,lin}}$  is even worse than  $R_{\text{erg,hyp,lin}}$ .

Consider also the rate region for one channel realization. The weighted sum and per-user rates for DPC can be obtained in a similar way to (61) and (62) using, e.g., a projected gradient algorithm [29], and for linear precoding using similarly the

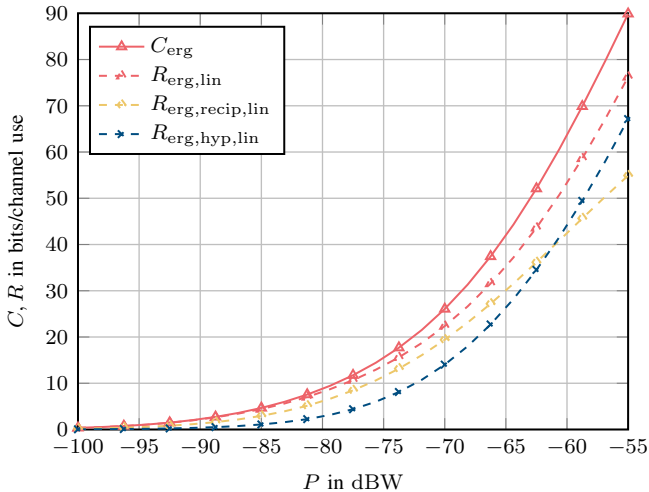


Fig. 13. Ergodic downlink sum rates for a UCA with 33  $\lambda/2$ -dipoles at the base station and two users with a 9  $\lambda/2$ -dipole UCA, all three with  $0.4\lambda$  antenna spacing, in a MU-MIMO i.i.d. channel.

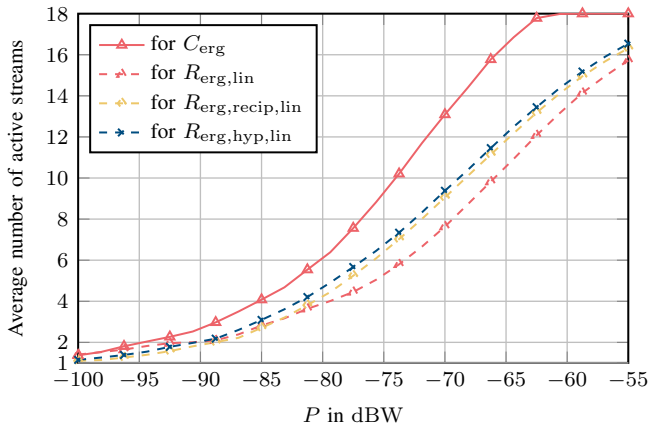


Fig. 14. Average number of active streams for a UCA with 33  $\lambda/2$ -dipoles at the base station and two users with a 9  $\lambda/2$ -dipole UCA, all three with  $0.4\lambda$  antenna spacing, in a MU-MIMO i.i.d. channel.

weighted sum rate maximization algorithm from [34]. When we have a look at the rate region for one channel realization in the same setting as for the sum rates, we can see a similar behavior as for the sum rate, see Fig. 12. The curves corresponding to the sum capacity and its corresponding sum rate with linear ZF precoding are called “cap” and “cap,lin” in the figure, and accordingly “hyp” and “hyp,lin” for the hypothetical sum rate and “recip,lin” for the one for the ordinary reciprocity relation. The performance using linear ZF precoding is very close to DPC.

#### D. MU-MIMO

For MU-MIMO, let us also consider a UCA with  $N = 33$  antennas at the base station and two mobiles with a UCA of 9 antennas, all three with  $0.4\lambda$  antenna spacing. For smaller transmit powers, the performance of linear ZF precoding is very close to DPC for the sum capacity and the hypothetical sum rate. But as the transmit power increases, the gap also increases, see Fig. 13. Similar to MU-MISO, for small  $P$ ,

$R_{\text{erg,recip,lin}}$  performs well, around  $P = -70$  dBW the gap to  $R_{\text{erg,hyp,lin}}$  starts to decrease considerably, at  $P \approx -61$  dBW they intersect and for even larger  $P$ ,  $R_{\text{erg,recip,lin}}$  starts to saturate. Compared to MU-MISO, the sum rate loss compared to  $C_{\text{erg}}$  increases for all ergodic rates, i.e., the loss increases with an increasing number of mobile antennas.

The average numbers of active streams in Fig. 14 show that for small transmit powers, they are very similar for DPC and linear ZF, but as the SNR increases, those for DPC increase much faster, i.e., the larger sum capacity and hypothetical rate in Fig. 13 can be explained by DPC supporting more active streams.

## VI. SIMULATIONS WITH THE QUADRIGA CHANNEL GENERATOR

QuaDRiGa [14], [15] is a channel generator written in MATLAB, which allows channels to be generated that are more realistic than i.i.d. channels. It is compatible with the current 3GPP channel model, 3GPP TS 38.901 [39], valid from 500 MHz to 100 GHz. As in [40], we consider a single non-sectorized base station site in the urban macrocell (UMA) model, but without mobility. The model assumes a hexagonal grid of cells with base station sites at certain corners of the hexagons. When the base station serves all mobiles closest to it, it serves a hexagon with edge length  $(500/\sqrt{3})$  m and is located at its center. The  $\lambda/2$ -dipoles at the base station and at the mobiles are all oriented vertically. The mobiles are distributed uniformly in the hexagon outside of a circle with radius 35 m around the base station. The altitude of the base station is 25 m and that of the mobiles is determined according to [39]. The continuous time channels obtained by QuaDRiGa need to be scaled by  $\text{Re}(Z_A)$  so that they fit the circuit-theoretical model and the receive power matches. Additionally, they need to be filtered by a transmit and a receive filter and sampled, since the QuaDRiGa continuous time channels are impulse trains for each individual channel between a transmit and a receive antenna. As in [40], we use root-raised cosine transmit and receive filters with  $\Delta f = 15$  kHz and roll-off factor 1 at the center frequency 3.5 GHz, because it does not introduce any noise correlations in time-domain after sampling. The bandwidth is similar to an LTE subcarrier. Regarding the noise parameters, the same parameters as for the i.i.d. channels are used, but the noise (co-)variances are scaled by 15/740, so they match the smaller bandwidth, maintaining the same noise power per bandwidth. We assume that the channel in discrete time is frequency flat, so the channel evaluated at  $\nu = 0$  Hz is [40]

$$\mathbf{Z}_{21} = \sum_{n_{\text{path}}=1}^{N_{\text{path}}} \mathbf{Z}_{21,n_{\text{path}}}, \quad (63)$$

where  $N_{\text{path}}$  is the number of paths of the QuaDRiGa channel and  $\mathbf{Z}_{21,n_{\text{path}}}$  are the coefficients corresponding to path  $n_{\text{path}}$ .

Let us now compare the simulation results for the SU-MISO and MU-MIMO scenarios in the i.i.d. channel with the one in the QuaDRiGa scenario. The attenuation of the channels generated by QuaDRiGa is larger than for the i.i.d. channel, so the ergodic (sum) rates are plotted for a larger  $P$  such that

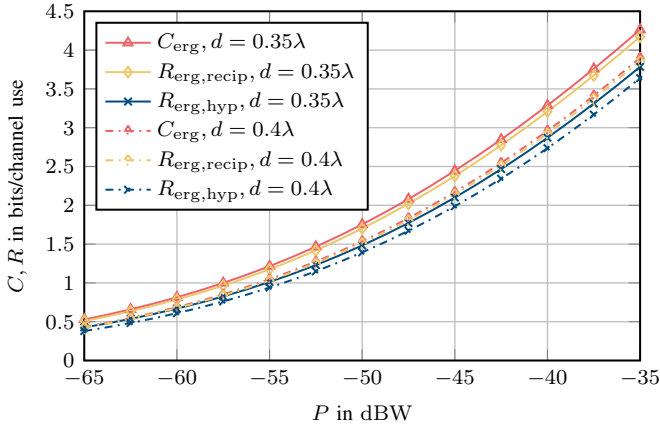


Fig. 15. Ergodic downlink rates for a UCA with 9  $\lambda/2$ -dipoles, and 0.35 $\lambda$  and 0.4 $\lambda$  antenna spacing in a SU-MISO QuaDRiGa channel.

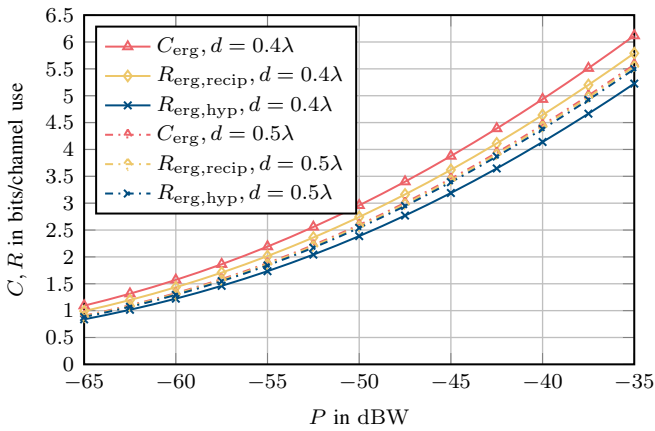


Fig. 16. Ergodic downlink rates for a UCA with 33  $\lambda/2$ -dipoles and 0.4 $\lambda$  and 0.5 $\lambda$  antenna spacing in a SU-MISO QuaDRiGa channel.

similar ergodic (sum) rates are achievable, see Figs. 15, 16 and 18. For SU-MISO in the range plotted, the slope of the ergodic rates is smaller than in the i.i.d. channel at a similar ergodic rate. This means that for many channel realizations, the channel attenuation is large and the slope of  $\log_2(1 + \text{SNR})$  is smaller than 1 in logarithmic scale. There is a similar rate loss if the base station uses the ordinary reciprocity relation as in the i.i.d. channel. Similarly,  $C_{\text{erg}}$  and  $R_{\text{erg, recip}}$  are larger for  $N = 33$  than for  $N = 9$ , and larger for smaller  $d$  than for larger  $d$ . Therefore, a smaller  $d$  is also advantageous and desirable here. Also similarly, on average less power is radiated than predicted if the base station uses conventional modeling. For  $d = 0.35\lambda$  and 0.4 $\lambda$ , the loss due to this and due to the suboptimal beamforming is smaller for the channels generated by QuaDRiGa, but for  $d = 0.5\lambda$ , they are about the same. This smaller loss for  $d = 0.35\lambda$  and 0.4 $\lambda$  corresponds to the distribution of  $\alpha$  being shifted a bit closer to 1, see Fig. 17. Furthermore, the variation of  $\alpha$  also gets slightly smaller for  $d = 0.35\lambda$  and 0.4 $\lambda$ , but larger for  $d = 0.5\lambda$ . As in the i.i.d. channel, using the ordinary reciprocity relation leads to higher ergodic rates than conventional modeling.

In the MU-MIMO scenario, the ergodic sum rates look similar as in the i.i.d. channels, see Figs. 13 and 18, but

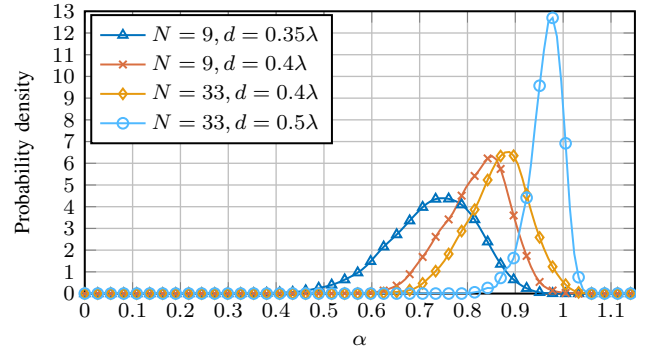


Fig. 17. Probability density of  $\alpha$  for a UCA for four scenarios in a SU-MISO QuaDRiGa channel.

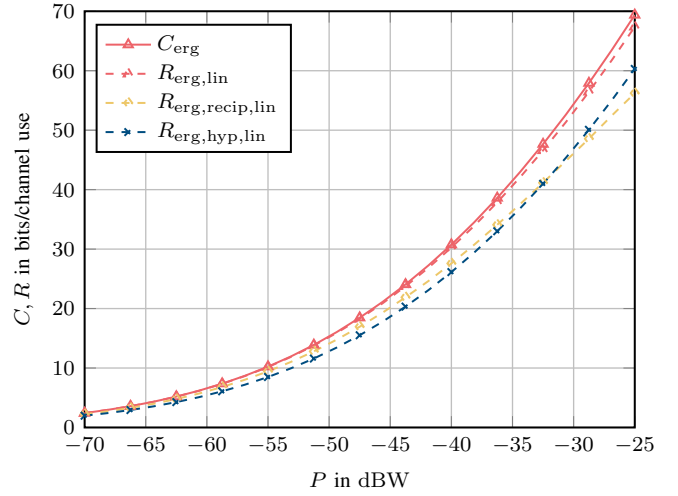


Fig. 18. Ergodic downlink sum rates for a UCA with 33  $\lambda/2$ -dipoles at the base station and two users with a 9  $\lambda/2$ -dipole UCA, all three with 0.4 $\lambda$  antenna spacing, in a MU-MIMO QuaDRiGa channel.

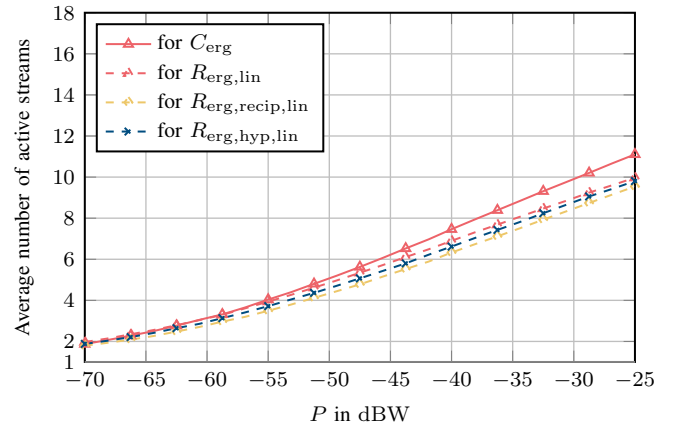


Fig. 19. Average number of active streams for a UCA with 33  $\lambda/2$ -dipoles at the base station and two users with a 9  $\lambda/2$ -dipole UCA, all three with 0.4 $\lambda$  antenna spacing, in a MU-MIMO QuaDRiGa channel.

the losses due to using the ordinary reciprocity relation or ignoring the coupling are smaller and linear ZF is closer to DPC. Regarding the average number of active streams, see Figs. 14 and 19, fewer are active for the same sum rate in the

QuaDRiGa channels than in the i.i.d. channels. This can be explained by the larger correlation of the QuaDRiGa per-user channels. Furthermore, the difference between the numbers of active streams for linear ZF and for DPC is smaller for the QuaDRiGa channels. As the linear ZF exploits cooperation between the antennas belonging to the same users using the SVD, the advantage of DPC is that it can remove inter-user interference. Due to the random placing of the users in the QuaDRiGa model, the channels to different users are almost orthogonal, so DPC is less beneficial than for the i.i.d. channel model.

## VII. CONCLUSIONS

We have analyzed the reciprocity of a MU-MIMO TDD system based on Multiport Communication Theory. We have seen that by incorporating the physical noise model and the power consistency, the ordinary (pseudo-physical) reciprocity relation between the information-theoretic up- and downlink channel does not hold in general – even if the noiseless relation between the transmit voltage sources and the receive load voltages is reciprocal. Instead, a physically consistent reciprocity relation holds. We have shown how the base station can achieve capacity using this relation when it computes the downlink channel from the uplink channel: namely, by using the power-coupling matrix it needs to know anyway to obtain the information-theoretic channel and by using a database of noise covariance matrices of the mobiles.

We have shown that when the base station uses the ordinary reciprocity relation, it will use suboptimal beamforming vectors and suboptimal power allocations that can significantly decrease the (sum) rate of the downlink, depending on the array geometry and on the type of antennas used. When the base station uses conventional modeling, i.e., if it ignores the coupling, there can also be a significant rate loss. Furthermore it cannot even predict the power it radiates accurately and the radiated power can vary greatly. In multi-user systems, using the ordinary reciprocity relation is similar to having a channel estimation error, which leads to intra-cell interference between different users. The loss in achievable rate when ignoring mutual coupling is larger for a reduced antenna spacing, but capacity increases at the same time. Compactness is therefore advantageous for better performance.

These conclusions hold both for i.i.d. channels and for channels based on the 3GPP TS 38.901 UMa model generated by QuaDRiGa. This highlights the importance of taking the mutual coupling into account, and its effects on the reciprocity in the information-theoretic channel. It is sensible to take it into account by using two matrix multiplications with matrices that can be determined offline at the design stage.

Although our numerical results are based on canonical minimum scattering antennas to enable an analytic calculation of the impedance matrices of the arrays, the analysis is not limited to these types of antenna elements. For other antenna elements, the impedance matrices must be computed numerically with an appropriate electromagnetic solver or must be measured. Similarly, although we have only provided numerical results for i.i.d. channels and 3GPP TS 38.901 UMa

channels, the approach presented is not limited to these types of channels.

## ACKNOWLEDGMENT

The authors would like to thank C. Mollén for asking inspiring questions motivating them to investigate this topic, and M. T. Ivrlač, who was the main author laying out the Multiport Communication Theory, which is the basis on which this work has been carried out. The authors would like to acknowledge the contributions of their colleagues in the Horizon 2020 project ONE5G (ICT-760809), although the views expressed in this contribution are those of the authors and do not necessarily represent the project.

## REFERENCES

- [1] E. G. Larsson, O. Edfors, F. Tufvesson, and T. L. Marzetta, “Massive MIMO for next generation wireless systems,” *IEEE Commun. Mag.*, vol. 52, no. 2, pp. 186–195, Feb. 2014.
- [2] M. Petermann, M. Stefer, F. Ludwig, D. Wübben, M. Schneider, S. Paul, and K.-D. Kammeyer, “Multi-user pre-processing in multi-antenna OFDM TDD systems with non-reciprocal transceivers,” *IEEE Trans. Commun.*, vol. 61, no. 9, pp. 3781–3793, Sep. 2013.
- [3] F. Kaltenberger, H. Jiang, M. Guillaud, and R. Knopp, “Relative channel reciprocity calibration in MIMO/TDD systems,” in *Proc. Future Netw. Mobile Summit*, Florence, Italy, Jun. 2010.
- [4] S. Bazzi and W. Xu, “A simple over-the-air hardware calibration procedure in TDD systems,” in *Proc. IEEE 27th Annu. Int. Symp. Personal Indoor Mobile Radio Commun. (PIMRC)*, Valencia, Spain, Sep. 2016, pp. 583–588.
- [5] J. Vieira, F. Rusek, and F. Tufvesson, “Reciprocity calibration methods for massive MIMO based on antenna coupling,” in *Proc. IEEE Global Telecommun. Conf. (GLOBECOM)*, Austin, TX, USA, Dec. 2014, pp. 3708–3712.
- [6] J. Vieira, F. Rusek, O. Edfors, S. Malkowsky, L. Liu, and F. Tufvesson, “Reciprocity calibration for massive MIMO: Proposal, modeling, and validation,” *IEEE Trans. Wireless Commun.*, vol. 16, no. 5, pp. 3042–3056, May 2017.
- [7] H. Wei, D. Wang, H. Zhu, J. Wang, S. Sun, and X. You, “Mutual coupling calibration for multiuser massive MIMO systems,” *IEEE Trans. Wireless Commun.*, vol. 15, no. 1, pp. 606–619, Jan. 2016.
- [8] M. T. Ivrlač and J. A. Nossek, “Toward a circuit theory of communication,” *IEEE Trans. Circuits Syst. I*, vol. 57, no. 7, pp. 1663–1683, Jul. 2010.
- [9] —, “The multiport communication theory,” *IEEE Circuits Syst. Mag.*, vol. 14, no. 3, pp. 27–44, Aug. 2014.
- [10] J. W. Wallace and M. A. Jensen, “Mutual coupling in MIMO wireless systems: A rigorous network theory analysis,” *IEEE Trans. Wireless Commun.*, vol. 3, no. 4, pp. 1317–1325, Jul. 2004.
- [11] C. Waldschmidt, S. Schulteis, and W. Wiesbeck, “Complete RF system model for analysis of compact MIMO arrays,” *IEEE Trans. Veh. Technol.*, vol. 53, no. 3, pp. 579–586, May 2004.
- [12] M. L. Morris and M. A. Jensen, “Network model for MIMO systems with coupled antennas and noisy amplifiers,” *IEEE Trans. Antennas Propag.*, vol. 53, no. 1, pp. 545–552, Jan. 2005.
- [13] C. P. Domizioli, B. L. Hughes, K. G. Gard, and G. Lazzi, “Noise correlation in compact diversity receivers,” *IEEE Trans. Commun.*, vol. 58, no. 5, pp. 1426–1436, May 2010.
- [14] S. Jaeckel, L. Raschkowski, K. Börner, L. Thiele, F. Burkhardt, and E. Eberlein, “QuaDRiGa – quasi deterministic radio channel generator, user manual and documentation,” Fraunhofer Heinrich Hertz Institute, Tech. Rep. Version 2.0.0-664, Aug. 2017.
- [15] S. Jaeckel, L. Raschkowski, K. Börner, and L. Thiele, “QuaDRiGa: A 3-D multi-cell channel model with time evolution for enabling virtual field trials,” *IEEE Trans. Antennas Propag.*, vol. 62, no. 6, pp. 3242–3256, Jun. 2014.
- [16] T. Laas, J. A. Nossek, S. Bazzi, and W. Xu, “On reciprocity of physically consistent TDD systems with coupled antennas,” in *Proc. 21st Int. ITG Workshop Smart Antennas (WSA)*, Berlin, Germany, Mar. 2017, pp. 377–382.
- [17] M. T. Ivrlač and J. A. Nossek, “A multiport theory of communications,” in *Proc. 8th Int. ITG Conference Source Channel Coding (SCC)*, Siegen, Germany, Jan. 2010.

- [18] —, “On physical limits of massive MISO systems,” in *Proc. 20th Int. ITG Workshop Smart Antennas (WSA)*, Munich, Germany, Mar. 2016.
- [19] S. A. Schelkunoff and H. T. Friis, *Antennas, Theory and Practice*. Wiley: New York, Chapman & Hall: London, 1952.
- [20] H. Rothe and W. Dahlke, “Theory of noisy fourpoles,” *Proc. IRE*, vol. 44, no. 6, pp. 811–818, Jun. 1956.
- [21] E. Biglieri, R. Calderbank, A. Constantinides, A. Goldsmith, A. Paulraj, and H. V. Poor, *MIMO Wireless Communications*, 1st ed. Cambridge University Press, 2007.
- [22] T. Laas, J. A. Nossek, S. Bazzi, and W. Xu, “On the impact of the mutual reactance on the radiated power and on the achievable rates,” *IEEE Trans. Circuits Syst. II, Exp. Briefs*, vol. 65, no. 9, pp. 1179–1183, Sep. 2018.
- [23] Z. Botev. (2015, Dec.) Kernel density estimator. Version 1.5.0.0. [Online]. Available: <https://www.mathworks.com/matlabcentral/fileexchange/14034-kernel-density-estimator>
- [24] Z. I. Botev, J. F. Grotowski, and D. P. Kroese, “Kernel density estimation via diffusion,” *Ann. Statist.*, vol. 38, no. 5, pp. 2916–2957, 2010.
- [25] E. Telatar, “Capacity of multi-antenna Gaussian channels,” *Eur. Trans. Telecommun.*, vol. 10, no. 6, pp. 585–595, Nov. 1999.
- [26] P. Viswanath and D. N. C. Tse, “Sum capacity of the vector Gaussian broadcast channel and uplink–downlink duality,” *IEEE Trans. Inf. Theory*, vol. 49, no. 8, pp. 1912–1921, Aug. 2003.
- [27] S. Vishwanath, N. Jindal, and A. Goldsmith, “Duality, achievable rates, and sum-rate capacity of Gaussian MIMO broadcast channels,” *IEEE Trans. Inf. Theory*, vol. 49, no. 10, pp. 2658–2668, Oct. 2003.
- [28] R. Hunger and M. Joham, “A general rate duality of the MIMO multiple access channel and the MIMO broadcast channel,” in *Proc. IEEE Global Telecommun. Conf. (Globecom)*, New Orleans, LO, USA, Nov./Dec. 2008.
- [29] R. Hunger, *Analysis and Transceiver Design for the MIMO Broadcast Channel*, ser. Foundations in Signal Processing, Communications and Networking. Springer: Berlin, Heidelberg, 2013, no. 8.
- [30] D. P. Bertsekas, “On the Goldstein-Levitin-Polyak gradient projection method,” *IEEE Trans. Autom. Control*, vol. AC-21, no. 2, pp. 174–184, Apr. 1976.
- [31] S. Yang and J.-C. Belfiore, “The impact of channel estimation error on the DPC region of the two-user Gaussian broadcast channel,” in *Proc. 43rd Annu. Allerton Conf. Commun. Control Comput.*, Monticello, IL, USA, Sep. 2005, pp. 1366–1372.
- [32] K. Eriksson, S. Shi, N. Vucic, M. Schubert, and E. G. Larsson, “Globally optimal resource allocation for achieving maximum weighted sum rate,” in *Proc. IEEE Global Telecommun. Conf. (Globecom)*, Miami, FL, USA, Dec. 2010.
- [33] H. Al-Shatri and T. Weber, “Achieving the maximum sum rate using D.C. programming in cellular networks,” *IEEE Trans. Signal Process.*, vol. 60, no. 3, pp. 1331–1341, Mar. 2012.
- [34] C. Guthy, W. Utschick, R. Hunger, and M. Joham, “Efficient weighted sum rate maximization with linear precoding,” *IEEE Trans. Signal Process.*, vol. 58, no. 4, pp. 2284–2297, Apr. 2010.
- [35] S. S. Christensen, R. Agarwal, E. de Carvalho, and J. M. Cioffi, “Weighted sum-rate maximization using weighted MMSE for MIMO-BC beamforming design,” *IEEE Trans. Wireless Commun.*, vol. 7, no. 12, pp. 4792–4799, Dec. 2008.
- [36] W. K. Kahn and H. Kurss, “Minimum-scattering antennas,” *IEEE Trans. Antennas Propag.*, vol. 13, no. 5, pp. 671–675, Sep. 1965.
- [37] W. Wasyliwskyj and W. K. Kahn, “Theory of mutual coupling among minimum-scattering antennas,” *IEEE Trans. Antennas Propag.*, vol. 18, no. 2, pp. 204–216, Mar. 1970.
- [38] B. Lehmeyer, M. T. Ivrlač, and J. A. Nossek, “LNA characterization methodologies,” *Int. J. Circuit Theory Appl.*, vol. 45, no. 9, pp. 1185–1202, Sep. 2017.
- [39] “Study on channel model for frequencies from 0.5 to 100 GHz,” 3GPP, TS 38.901, Jun. 2017, Version 14.1.0.
- [40] T. Laas, J. A. Nossek, S. Bazzi, and W. Xu, “On the impact of the mutual impedance of an antenna array on power and achievable rate,” in *Proc. 22nd Int. ITG Workshop Smart Antennas (WSA)*, Bochum, Germany, Mar. 2018.